Implementation of a machine learning technique for estimating gamma direction using a coaxial High Purity Germanium detector

R. W. Gladen*[1], T. J. Harvey[2,3], S. S. Chirayath[2,3], A. J. Fairchild[1], A. R. Koymen[1], A. H. Weiss[1], V. A. Chirayathǂ[1]

[1]*Department of Physics, University of Texas at Arlington, Arlington, TX, USA 76019*

[2]*Center for Nuclear Security Science & Policy Initiatives, Texas A&M University, College Station, TX 77843-3473, USA*

[3]*Department of Nuclear Engineering, Texas A&M University, College Station, TX 77843-3133, USA*

ǂCorresponding author e-mail: chirayat@uta.edu

*Corresponding author e-mail: randall.gladen@uta.edu

Abstract

We demonstrate the ability to obtain the direction of the gamma rays using a standard coaxial high purity germanium (HPGe) detector using the direction-sensitive information embedded in the shape of the pre-amplified HPGe signals. We deduced the complex relationship between the shape of the signal and the direction from which the gamma-ray enters the detector active volume using a two-step machine learning technique. In the first step, we collected pulses from the HPGe detector due to a ^{133}Ba source placed in four distinct positions around the detector while keeping the distance from the center of the detector crystal constant. A subset of the pulses collected with radioactive source kept at the four positions was used to train an artificial neural network (ANN) called a self-organizing map (SOM) to cluster the HPGe waveforms based on their shape. The trained SOM network was then utilized to produce direction-specific maps corresponding to pulses generated when the ^{133}Ba source is at a specific location with respect to the detector. In the second step, we used the SOM-generated direction-specific maps to train another network composed of a single feedforward layer for predicting the direction of the gamma photon from the pulses produced by the HPGe detector because of the gamma energy deposition. Our results show that even without employing complex methodologies, a standard coaxial HPGe detector can estimate the direction of incoming gamma rays and thus, provide initial guidance on the gamma-emitting radioactive source direction with reference to the detector.

1. Introduction and Background

Typical radiation detectors used in search procedures for obscured radioactive materials include commonplace and well-characterized detectors that can detect alpha, beta, gamma rays, or neutrons emissions. Neutron and gamma-ray detection are generally more applicable for source search due to those radiation types' longer mean free paths. Detectors like end-window Geiger-Mueller (G-M) tubes or compact scintillator detectors are most commonly used in searches due to their mobility and sensitivity to various particle types [1]. Detectors used in source searching commonly rely on count rate changes with source-to-detector distance to physically locate the material. These detectors are widely used in source search applications during which the count rate is monitored as the detector's spatial location is varied. This technique can generate a field of dose rates that can infer the most likely spatial location or a sought-after source since count rates are more likely to increase in areas nearer to the radioactive material. Alternatively, a user of a mobile detector can appropriately adjust their searching path as they see the count rate change with their spatial position. These methods can effectively track down lost or hidden sources but feature some drawbacks. Count rate search methods can be time-consuming if the search area is large and there is no initial guidance on the source direction. Count rate methods can also be limited by difficult terrain or inaccessible areas. Spatial radiation surveys also typically do not feature a vertical height component on 2-D count rate maps, leaving ambiguity concerning the position of potential radioactive material on upper floors of buildings or below ground.

Detection systems that have sought to resolve some of these problems include radiation imaging detectors such as coded aperture systems [2,3], Compton-scatter cameras [4], neutron-scatter cameras [5], and time projection chambers [6]. These detectors provide directional and spatial data along with count rate and spectroscopic data. Imaging detectors can also perform rough imaging of the size and shape of radioactive material close to the detector systems. Compton scatter cameras are already widely used in medical imaging applications, and compact, mobile designs have been demonstrated in source searching applications. Compact neutron-scatter camera systems have also been proposed as detectors to perform source searching. Because of their relatively large size, high complexity, and required particle flux, time projection chambers and coded aperture systems have not been proposed as possible source localizers except in minimal scenarios. Though imaging systems provide a plethora of spatial data that could be valuable in source searching, they also feature many drawbacks. Compact imaging systems tend to be much more expensive than G-M tubes and simple scintillators due to multiple detector volumes, complex photoelectronic readouts, and computationally taxing post-processing needs. In many cases, imaging systems may be overengineered for source localization since what is sought in that application is the general direction of nearby sources rather than the level of detail yielded by a complete image. These facts point toward the usefulness of a simple source-direction-pointing detector intermediate in complexity between directionality "blind" standard detectors and more complex imaging detectors.

Several detector designs have been proposed to "point" towards a nearby radiation source. These detectors broadly can be grouped into three classes: spectral comparison-type systems, count rate occlusion-type systems, and multi-channel readout-type systems. Fig. 1 demonstrates the general operating principle of each of these detector types. Spectral comparison-type systems use multiple types of scintillator materials in a single system. The spatial arrangement of each scintillator relative to the position of a nearby radiation source will result in differential feature prominence in the characteristic spectra produced by each material. This type of directional detector has been little explored since its initial proposal as a passive directional monitor of radiation release events [7], though it does allow for direction detection using only a single photomultiplier tube (PMT). Much more widely prototyped are occlusion-type detectors. These systems rely on differential count rates attained from separate detector volumes. The detector volumes are arranged so that volumes nearer to a radiation source will record the highest count rate while simultaneously occluding the radiation flux arriving at the other detector volumes and depressing their count rates via the "shadow effect." The real-time differential count rates determined by the detector system can be used to estimate the direction of a stationary source or track the movement of a mobile source. Occlusion-type systems may or may not use shielding in addition to the detector volumes and may operate in a stationary position or may be rotated around a central axis to better estimate source positions. Occlusion-type detectors have been well explored in the literature [8-17]. The third general class of simple directional detectors uses a single detector volume coupled to pixelated or otherwise distributed photodetectors. In these systems, source direction is estimated by observing the differential response across all data channels. The channels closer to or oriented towards the radiation source will generally show a more significant response. The concept behind these detectors is similar to occlusion-type systems, though they allow for more compact designs by removing the need for multiple detector volumes. Several examples of purpose-built non-imaging multi-channel readout directional detectors have been demonstrated [18, 19], though pixelated single volume detectors can often also act as imagers.

Simple directional detector systems need not be purpose-built: Many detectors initially designed for standard spectroscopic capabilities may provide spatial information if the signals change when the source position is altered. During typical measurements with an HPGe system, it was observed that the average signal characteristics of collected pulses varied with the positioning of the radioactive source with reference to the detector. This is not surprising as the shape of the pre-amplified HPGe signals depend critically on (i) the point of interaction of the γ photon in the detector, (ii) the number of interactions per γ photon, and (iii) the carrier transport dynamics across the electrodes. Thus, standard HPGe detectors with asymmetrical geometry have directionally sensitive information buried in the signals to act analogously to the purpose-built occlusion or pixelated directional detectors. Therefore, we can use a standard asymmetric semiconductor detector to infer the direction of a nearby gamma source if we can deduce the complex relationship between the radiation source position, the average intra-detector particle interaction location, and the shape of the detector voltage pulses.

Advancements in Artificial Intelligence and machine learning algorithms have made it possible to derive complex relationships from data that are difficult to obtain using conventional methods and, therefore, have found increasing application in all aspects of nuclear physics experiments [20, 21]. Machine learning methods have been successfully integrated with directional detectors that incorporate multi-channel readout [19] or employ separated scintillation volumes [22]. Our group recently employed unsupervised machine learning to cluster HPGe pulses according to their shape and derived the most suitable shape-dependent discrimination parameters for obtaining the time information. By employing the shape-dependent "variable fraction discrimination" method, we could bring the timing resolution of an HPGe detector down to a few nanoseconds without rejecting any signals [23]. Here we employ a similar strategy to cluster HPGe detector pulse shapes using a SOM network to obtain a map related to the gamma entry direction. We further train a second network with a single feedforward layer to deduce the relationship between the direction-specific SOM-generated map and the source position. Our results show that we can estimate the general direction of the gamma source with a standard coaxial HPGe detector with good reliability. Combined with the superior energy resolution of an HPGe detector, our method converts a standard HPGe detector into an effective tool for searching and identifying nuclear and radiological materials.

2. Monte Carlo Simulations

We used a Monte Carlo model of an HPGe detector system to confirm the relationship between the source position with reference to the detector volume and the intra-detector interaction position. The model's cells, surfaces, and materials were set according to the manufacturer specifications of an Ortec GEM-10195 detector. Fig. 2 shows an axial and radial view of the simulation model of the active detector volume, cold finger, and surrounding layers. The geometric model was run in MCNPX-PoliMi, a Monte Carlo code helpful in examining the details of individual interaction events rather than tallies. MCNP-PoliMi can output the 3-D interaction position, energy deposition, and timing values for particles interacting in cells of interest. Using the capabilities of MCNPX-PoliMi, we simulated the positions at which the gamma photon deposits its energy in the active detector volume as a function of the azimuthal position of a ^{133}Ba point with reference to the center of the active detector volume. The source was placed 25 cm from the center of the detector volume for the simulations to match the measurement conditions as shown in Fig. 3. A total of 10 million decay histories were simulated at each position. We confirmed the ability of the simulation in MCNPX-PoliMi to accurately represent our detector system and experiment by comparing the experimental energy spectrum to the one produced by the simulation (Fig. 4). Here we applied a standard MCNP F8 energy deposition tally with Gaussian peak broadening to the simulated detector cell consisting of the HPGe material. The simulated energy spectrum compares favorably with the experimental gamma energy spectrum. Please note that instrumental broadening of the gamma peaks was included in the simulation using empirical parameters (a, b & c) obtained by fitting the variation of the full width at half maximum (FWHM) of the experimental gamma peaks with the gamma energy (E) using the equation $a + b\sqrt{E + cE^2}$.

The MCNPX- PoliMi output file containing the spatial positions of each interaction in the active volume was saved at each source position. Fig. 5 shows 3-D scatter plots of the saved interaction positions within the cylindrical detector volume for four source positions. Only 10,000 interactions are shown in each plot for clarity. The scatter plots clearly show that the interaction positions tend to cluster close to the surfaces nearer to the source for the gamma energies used in the simulation. Based on the scatter plots, it is evident that the charge carriers (electrons and holes) generated by the gamma travel have different transport paths to the respective electrodes, ultimately leading to different pulse shapes. Fig. 6 shows the distributions in interaction position in the x and y directions for the ^{133}Ba point source at positions 0, 45, 90, and 180 azimuthal degrees from the front face of the detector active volume. The changes in interaction position distribution with source spatial position show that the coaxial HPGe detector can infer the average interaction position and thus the general source direction by calculating the average charge carrier travel time from the position of interaction in the axial direction to the point of charge collection. We achieve this using machine learning capabilities, allowing us to bypass complex charge transport modeling [25, 26] or segmentation of coaxial HPGe detectors [27].

3. Methods

The data needed for training and testing the two-step machine learning algorithm was collected using a coaxial HPGe detector system consisting of a single p-i-n (p-n junction with an intrinsic region) region and readout (i.e., not segmented). The details of the data collection, curation prior to training, and the network architectures employed are discussed below.

3.1 Apparatus

Detector pulses from a coaxial Ortec GEM HPGe detector were obtained by placing a one microcurie ^{133}Ba source at 25 cm from the center of the detector crystal along its axis, as shown in Fig. 3. At this initial position, ~200,000 pulses were collected with a Lecroy HDO with a 12-bit resolution and a sampling rate of 2.5 GS/s. Following this collection, the source was moved to the 90° position (with respect to the detector axis) and then to the 180° position—kept at a constant distance of 25 cm from the crystal center—and ~200,000 pulses were collected for each direction. Finally, the source was moved to the 45° position, and another 100,000 pulses were collected. Due to the inherent asymmetry of the detector, the voltage pulses generated by the detector with the source at different directions are expected to have distinguishable features. There are several methods for clustering pulses together with similar features. The most straightforward and visually interpretable is the self-organizing map (SOM) [23]. It should be noted for clarification that the direction of the source is not estimated from a single interaction event, but from a distribution of events whose mean position in the active detector volume determines the shape of the pulse. This information is reduced in dimensionality by the self-organizing map.

3.2 Self-organizing map

The digitized pre-amplified pulses were analyzed and cleaned using the software described in [24]. Following this, we created a single data set using 10,000 pulses from the 0°, 90°, and 180° positions and 5,000 pulses from the 45° source (i.e., a data set consisting of 35,000 pulses).

The data set had all types of pulses, including saturated and noisy pulses, as in Fig. 7, which shows a small subset of voltage pulses used. The amplitude normalized data set was used to train the SOM, an unsupervised neural network that reduces the input space by grouping similar pulses together [28]. The training was done using the SOM algorithm provided in the Deep learning toolbox of MATLAB® [29]. The trained SOM consisted of 12 ×12 neurons connected in a hexagonal topology. The SOM was trained for 2000 iterations, and the resulting sample hits plot from the training is given in Fig. 8. Fig. 8 shows the result of shape-based pulse clustering with the number of pulses associated with each of the 144 neurons shown. The trained SOM network was then used to produce direction-specific maps similar to Fig. 8, but for voltage pulses produced by gamma entering the detector from one direction. We created two data sets (each consisting of both training and testing data subsets) comprised of either (i) one thousand or (ii) one hundred pulses acquired with the ^{133}Ba source at a specific position to feed into the trained SOM network. The network now produces maps characteristic of the position of the source about the detector. Fig. 9 is a sample of direction-specific maps produced using an input data set with one thousand detector pulses. To emphasize the direction specificity of these maps, we show in Fig. 10 the pulses corresponding to the neuron with the highest number of hits (or highest number of pulses) in the direction-specific maps shown in Fig. 9. The fact that gamma entering the detector from different directions produces pulses with visibly different shapes shows that even a standard coaxial HPGe detector can be used as a direction-sensitive detector with pulse clustering and analysis. These direction-specific maps are represented as one-dimensional 144-length vectors with the number of hits represented as integer entries and the neuron represented by the vector index. Since we took only one thousand (or one hundred) input pulses at a time from the data that was not used in the initial training, multiple vectors were produced corresponding to each direction. These vectors were labelled according to the source direction (0° (0), 45° (1), 90°, (2), and 180° (3)), resulting in four distinct classes.

3.3 Prediction model

We trained a model composed of a single feedforward layer with a ReLU activation to predict the direction of the source. The direction-specific 144-length vectors generated using the trained SOM network for the different positions of the ^{133}Ba source were the input to the second network for direction prediction. Other machine learning algorithms were tested, including decision trees and support vector machines, but only the neural network architecture met the requirements of high accuracy on the test set while also producing reasonable accuracy on a second test set composed of a "mixture" of vectors, as described in Section 4.1. It needs to be emphasized that the simple feedforward network was suitable for the present experiment as we are trying to distinguish between pulses collected only from four source locations around the detector. In a more comprehensive experiment that includes many source locations and a larger SOM architecture, such a simple network may no longer be sufficient. Our aim here is to present a proof of concept for a method using pulse clustering algorithms (the SOM in our case) in the analysis of determining the location of radioactive sources.

The model was developed and trained using the PyTorch library. The dimension of the feedforward layer was 144 (the same dimension as the input vectors). The model was trained in two different ways to test the feasibility of applying the methodology with limited data for training or during testing. The training was performed using direction-specific vectors generated using SOM taking 1000 input pulses in one method. In a second way, the network was trained with direction-specific vectors generated using SOM taking 100 input pulses. Similarly, the testing was done with SOM vectors generated with 1000 or 100 input pulses. For the method that used 1000-input pulses for both training and testing, the training and testing accuracies were 100% (the confusion matrix for this set is given in Figure 10(a)), and for the 100-pulse training & testing method, the training and testing accuracies were 94.5% and 72.5%, respectively (see Fig. 11(b) for the confusion matrix). The total number of vectors used in training was 671 (or 6710) for SOM vectors produced with 1000 (or 100) vectors each, with 10% set aside for testing. The accuracy of the prediction algorithm depends on the size (number of vectors used to train the prediction model) and the density (number of pulses per SOM used to generate the vectors) of the data, which has been discussed in the next section.

4. Results and Discussion

4.1 Mixture of directions

To test the ability of our algorithm to predict the direction of gamma rays with our limited dataset, we combined random SOM vectors (from the test set; these vectors were not exposed to the algorithm during training) two at a time and provided the resulting vector to the network for prediction. The prediction accuracy was measured by the probabilities generated by the final activation function (softmax). This output consists of four values that give the probability that the source is in one of the four locations. If the two highest probabilities of the softmax activation function corresponded to the correct locations of the source, the prediction was labeled as correct (for testing with SOM vectors from a single direction, only the maximum probability was considered). The network successfully predicted the components in this way with ~70% accuracy on the 1000-pulse set (training & testing). In addition to the original test set accuracy, the reasonable accuracy provided by this method indicates that the network is learning the patterns produced by the SOM and not simply memorizing the data. An application of this method may allow the detection of multiple radiation sources in different locations, provided the total count rate does not lead to shape variations due to pulse pile-up.

4.2 Training and Testing Variations

An additional test of the algorithm was the variation of the amount of information contained in each SOM vector to answer the following question: Is it better to train the feedforward network on *more* data (size) with *fewer* pulses per SOM (density) or *less* data with *more* pulses per SOM? Each SOM prediction vector was produced by feeding the SOM network 1000 pulses in the initial training and testing method for the feedforward network. This results in fewer total SOM vectors, as more pulses are used to produce each vector. We obtained the best results (100% accuracy) when training and testing were performed with SOM vectors was produced with 1000 pulses (Fig. 11(a)). Another option is to reduce the number of pulses used to create each SOM vector. Doing so will result in more total SOM vectors with which to train & test the feedforward prediction network. Reducing the number of pulses in each map to 100 for both training and testing resulted in a testing accuracy of ~ 72.5%, as stated earlier (Fig. 11(b)). However, keeping the training set at 1000 pulses per SOM vector and reducing only the testing set to 100 pulses per SOM resulted in a reduced test set accuracy of ~ 67.5%. The confusion matrix for this result is given in Fig. 11(c). Using a training set consisting of 100 pulses per SOM vector and a test set that consisted of 1000 pulses per map resulted in training and test set accuracies of ~ 94.5% and ~ 80%, respectively (confusion matrix in Fig. 11(d))—an improvement compared to the 100-pulse test set. Our results suggest that a denser testing set leads to better accuracy. With more pulses per map, the SOM network may be able to recognize the direction-specific patterns better even though there were fewer total maps with which to train.

5. Conclusions

We have shown the feasibility of acquiring source position information from coaxial HPGe detectors using a combination of unsupervised and supervised machine learning algorithms. The results we have presented were using data obtained under ideal conditions for gamma energies generated by a ^{133}Ba source. Further work—in particular, the collection of a larger dataset consisting of a significantly larger variety of directions, distances from the detector, and source isotopes—is needed to select the appropriate size of the SOM network and depth of the neural network required for use in the field. Applications of this technique may include implementation into handheld/portable coaxial HPGe detectors, which may be able to provide not only a high-resolution gamma spectrum but indicate a general direction from which the gamma rays are originating. Other applications include extracting the components in experimental data due to gamma originating away from the direct field of view. For example, there is an appreciable background in time-of-flight spectroscopy of electrons generated by positrons due to the electrons being correlated with delayed gamma produced by ortho Positronium (o-Ps) annihilation [30, 31]. Because of its long lifetime, o-Ps travel tens of centimeters away from the sample before annihilation. This causes the annihilation gamma to enter the detector active volume from positions away from the sample. We aim to implement the present algorithm to extract the component of the time-of-flight spectrum associated with gamma photons originating away from the sample, allowing us to study o-Ps formation in more detail.

Acknowledgments

A.H.W, A.R.K and V.A.C gratefully acknowledge the support of the National Science Foundation, USA (CHE-2204230). A. H. W gratefully acknowledge the support of the Welch Foundation, USA (Y-1968-20180324). A.H.W and A.R.K gratefully acknowledge the support of the National Science Foundation, USA (DMR-1338130 & DMR-1508719). S. S. C and T. J. H gratefully acknowledge the support of the Stanton Foundation.

References

1. International Atomic Energy Agency, Methods to identify and locate spent radiation sources, Vienna, 1995. Available at: https://www-pub.iaea.org/MTCD/Publications/PDF/te_804_prn.pdf (accessed on November 15th, 2021).
2. M. J. Cieślak, K. A. A. Gamage, R. Glover, "Coded-aperture imaging systems: Past, present and future development – A review", *Radiation Measurements*, *92*, 59 –71 (2016).

3. L. J. Schultz, et al., “Hybrid coded aperture and Compton imaging using an active mask”, *Nuclear Instruments and Methods in Physics Research Section A: Accelerators, Spectrometers, Detectors and Associated Equipment*, *608,* 267-274 (2009).
4. Anthony Sweeney "Compton imaging for homeland security", PhD dissertation, University of Liverpool, 2014.
5. T. Harvey, E. Andreas, K. Bachner, "Applications and Deployment of Neutron Scatter Cameras in Nuclear Safeguards Scenarios", *Journal of Nuclear Materials Management* , *48*, 4-21 (2020).
6. I. Jovanovic, N. S. Bowden, G. P. Carosi, M. Heffner, C. Roecker. "Neutron Time Projection Chamber for Nuclear Security and Verification Applications" *AIP Conference Proceedings*, *1412*, 370-376 (2011).
7. Y. Shirakawa, “Development of a direction-finding gamma-ray detector”, *Nuclear Instruments and Methods in Physics Research Section B: Beam Interactions with Materials and Atoms*, *263,* 58-62 (2007).
8. J. Uher, C. Frojdh, J. Jakubek, S. Pospisil, G. Thungstrom, Z. Vykydal, “Directional radiation detector”, *2007 IEEE Nuclear Science Symposium Conference Record,* 1162-1165 (2007).
9. G. L. Randall, E. Iglesis, H. F. Wong, R. S. Speller, “A method of providing directionality for ionising radiation detectors — RadICAL” *Journal of Instrumentation*, *9,* P10011 (2014).
10. D. Hanna, L. Sagnières, P. J. Boyle, A. M. L. MacLeod, “A directional gamma-ray detector based on scintillator plates”, *Nuclear Instruments and Methods in Physics Research Section A: Accelerators, Spectrometers, Detectors and Associated Equipment*, *797,* 13-18 (2015).
11. B. Ayaz-Maierhafer, C. G. Britt, A. J. August, H. Qi, C. E. Seifert, J. P. Hayward, “Design optimization for a wearable, gamma-ray and neutron sensitive, detector array with directionality estimation”, *Nuclear Instruments and Methods in Physics Research Section A: Accelerators, Spectrometers, Detectors and Associated Equipment*, *870,* 131-139 (2017).
12. A. Farzanehpoor Alwars, F. Rahmani, “Development of a high-precision gamma-ray source finder based on a single detector”, *Sensors and Actuators A: Physical*, *300,* 111633 (2019).

13. A. Guckes, A. Barzilov, P. Guss, "Directional detection of neutrons and photons using elpasolites: Computational study", Radiation *Measurements*, *124,* 127-131 (2019).
14. R. J. Olesen, B. E. O'Day, D. E. Holland, L. W. Burggraf, J. E. Bevins, "Characterization of novel rotating scatter mask designs for gamma direction identification", *Nuclear Instruments and Methods in Physics Research Section A: Accelerators, Spectrometers, Detectors and Associated Equipment*, *954,* 161232 (2020).
15. J. F. Liang, K. Talley, "Enhanced directional detection of gamma sources", *Nuclear Instruments and Methods in Physics Research Section A: Accelerators, Spectrometers, Detectors and Associated Equipment*, *1002,* 165304 (2021).
16. C. Britt, X. Wen, H. Qi, J. P. Hayward, "Directionality for wearable, closely packed radiation detector arrays", *Nuclear Instruments and Methods in Physics Research Section A: Accelerators, Spectrometers, Detectors and Associated Equipment*, *986,* 164708 (2021).
17. B. Egner, D. E. Holland, L. W. Burggraf, J. E. Bevins, "Development of a modular mixed-radiation directional rotating scatter mask detection system", *Nuclear Instruments and Methods in Physics Research Section A: Accelerators, Spectrometers, Detectors and Associated Equipment*, *987,* 164820 (2021).
18. R. Wang, et al., "Absolute Gamma Source Positioning with Position-sensitive Scintillation Detector Arrays", *2018 IEEE Nuclear Science Symposium and Medical Imaging Conference Proceedings (NSS/MIC),* 1-4 (2018).
19. L. Buonanno, D. di Vita, M. Carminati, C. Fiorini, "A Directional Gamma-Ray Spectrometer with Microcontroller-Embedded Machine Learning", *IEEE Journal on Emerging and Selected Topics in Circuits and Systems*, *10,* 433-443 (2020).
20. A. Boehnlein, et al. Artificial Intelligence and Machine Learning in Nuclear Physics. arXiv:2112.02309 (2021).
21. R. W. Gladen, et al., "Neural Assessment of Non-Destructive Assay for Material Accountancy, *INMM Annual Meeting proceedings* (2021) (https://resources.inmm.org/annual-meeting-proceedings/neural-assessment-non-destructive-assay-material-accountancy).
22. M. Durbin, R. Sheatlsey, P. McDaniel, A. Lintereur, "A Multi-Step Machine Learning Approach to Directional Gamma Ray Detection", *2020 IEEE Nuclear Science Symposium and Medical Imaging Conference (NSS/MIC)*, 1-3 (2021).

23. R.W. Gladen, V. A. Chirayath, A.J. Fairchild, M. T. Manry, A. R. Koymen, A. H. Weiss, "Efficient machine learning approach for optimizing the timing resolution of a high purity germanium detector", *Nuclear Instruments and Methods in Physics Research Section A: Accelerators, Spectrometers, Detectors and Associated Equipment, 981*, 164505 (2020).
24. R.W. Gladen, V.A. Chirayath, A.J. Fairchild, A.R. Koymen, A.H. Weiss, "Digital methods for the coincident measurement of the energies of positron-induced electrons and Doppler-shifted annihilation gamma quanta", *Nuclear Instruments and Methods in Physics Research Section A: Accelerators, Spectrometers, Detectors and Associated Equipment, 953,* 162887 (2019).
25. B. Bruyneel, P. Reiter, G. Pascovici, "Characterization of large volume HPGe detectors. Part I: Electron and hole mobility parameterization", *Nuclear Instruments and Methods in Physics Research Section A: Accelerators, Spectrometers, Detectors and Associated Equipment, 569,* 764–773 (2006).
26. L. Mihailescu, W. Gast, R.M. Lieder, H. Brands, H. JaKger, "The influence of anisotropic electron drift velocity on the signal shapes of closed-end HPGe detectors", *Nuclear Instruments and Methods in Physics Research Section A: Accelerators, Spectrometers, Detectors and Associated Equipment, 447*, 350-360 (2000).
27. T. Niedermayr, K. Vetter, L. Mihailescu, G.J. Schmid, D. Beckedahl, J. Blair, J. Kammeraad, Gamma-ray imaging with a coaxial HPGe detector, *Nuclear Instruments and Methods in Physics Research Section A: Accelerators, Spectrometers, Detectors and Associated Equipment, 553,* 501–511 (2005).
28. T. Kohonen, The self-organizing map. *Proceedings of the IEEE*, *78,* 1464-1480 (1990).
29. The Mathworks Inc., Deep learning toolbox: User's guide (R2020a), 2020, Retrieved from www.mathworks.com/help/deeplearning/ug/cluster-with-selforganizing-map-neural-network.html.
30. Shuping Xie, "Positron Annihilation Induced Auger Electron Spectroscopy of Inner Shell Transitions Using Time of Flight Technique", PhD dissertation, University of Texas at Arlington (2002).
31. V. A. Chirayath, et al., "Modeling Positronium induced background in the time-of-flight (TOF) spectra of positron induced secondary electrons using Monte Carlo methods", *APS March Meeting 2022,* March 14–18, 2022; Chicago.

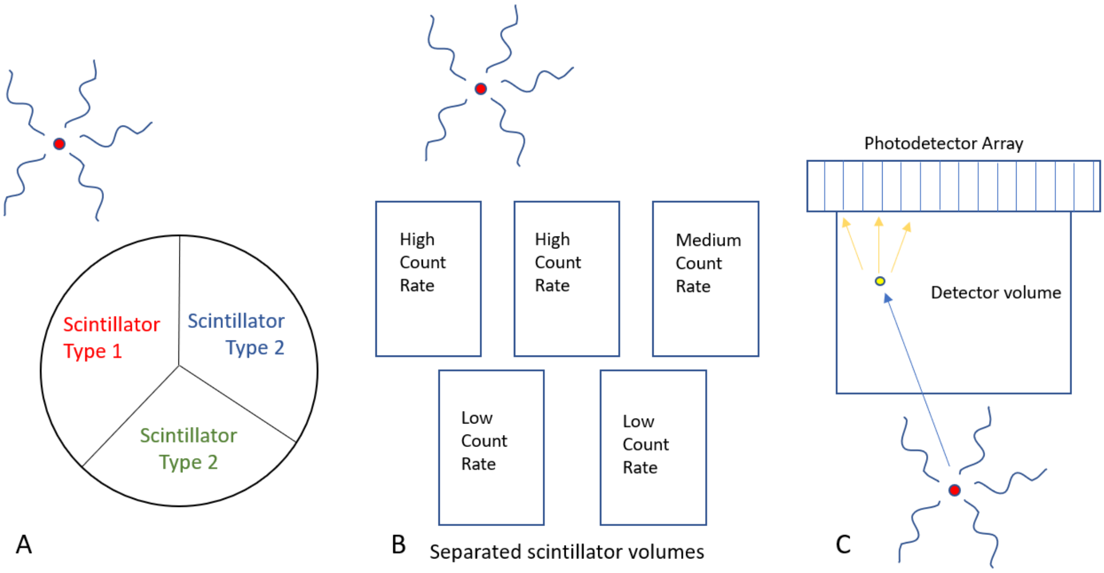

Fig. 1 Three general concepts for scintillator-based, non-imaging directional detectors. Type A uses the relative prominences of the peaks corresponding to each of the three scintillator types estimate the radial direction of the source. Type B infers the source direction through the differential count rates generated in separate scintillator volumes and their spatial arrangement. Type C estimates the source direction by comparing which channels in a multi-channel photomultiplier system coupled to the detector volumes receive the most light during a series of scintillation events.

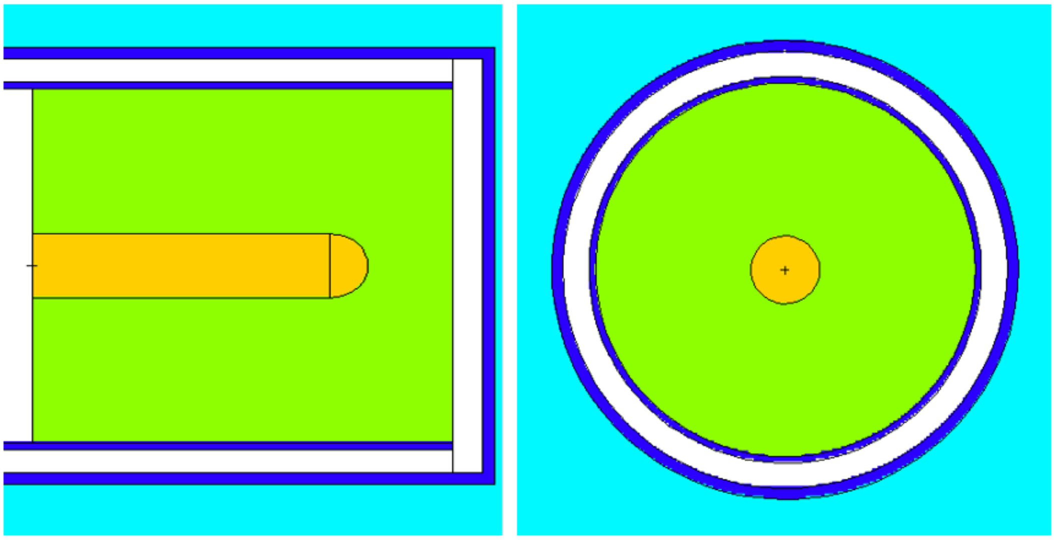

Fig. 2 MCNPX-PoliMi model of the simulated detector. The green region is the HPGe crystal, the yellow regions is the copper cold finger, the dark blue regions are aluminium and mylar casing and structural material, and the white and light blue regions are air.

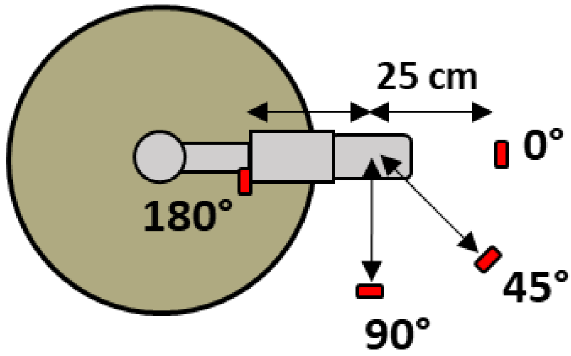

Fig. 3 Experimental geometry showing the position of the ^{133}Ba source. Each position was placed 25 cm from the center of the crystal, which is also the distance between the back of the detector electronics shroud and the center of the crystal. The digitally collected pulses were analyzed using the internally developed software to generate the energy spectrum [24].

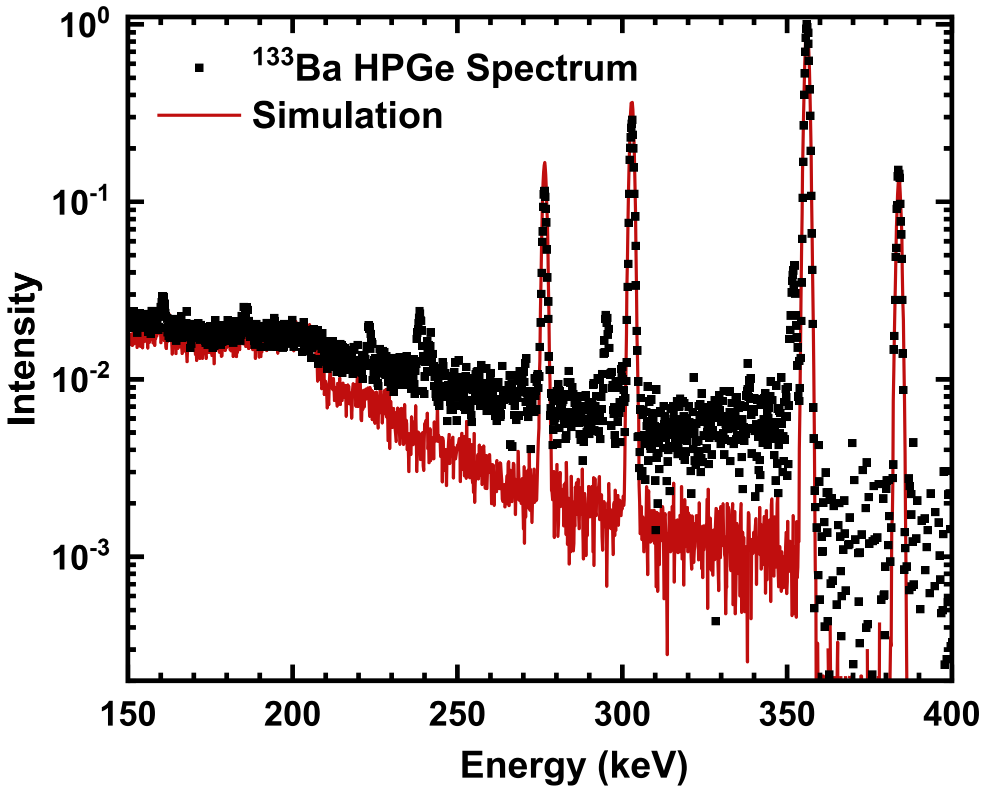

Fig. 4 The background subtracted experimental (red) and simulated (black) 133Ba spectra, including all four positions of the source.

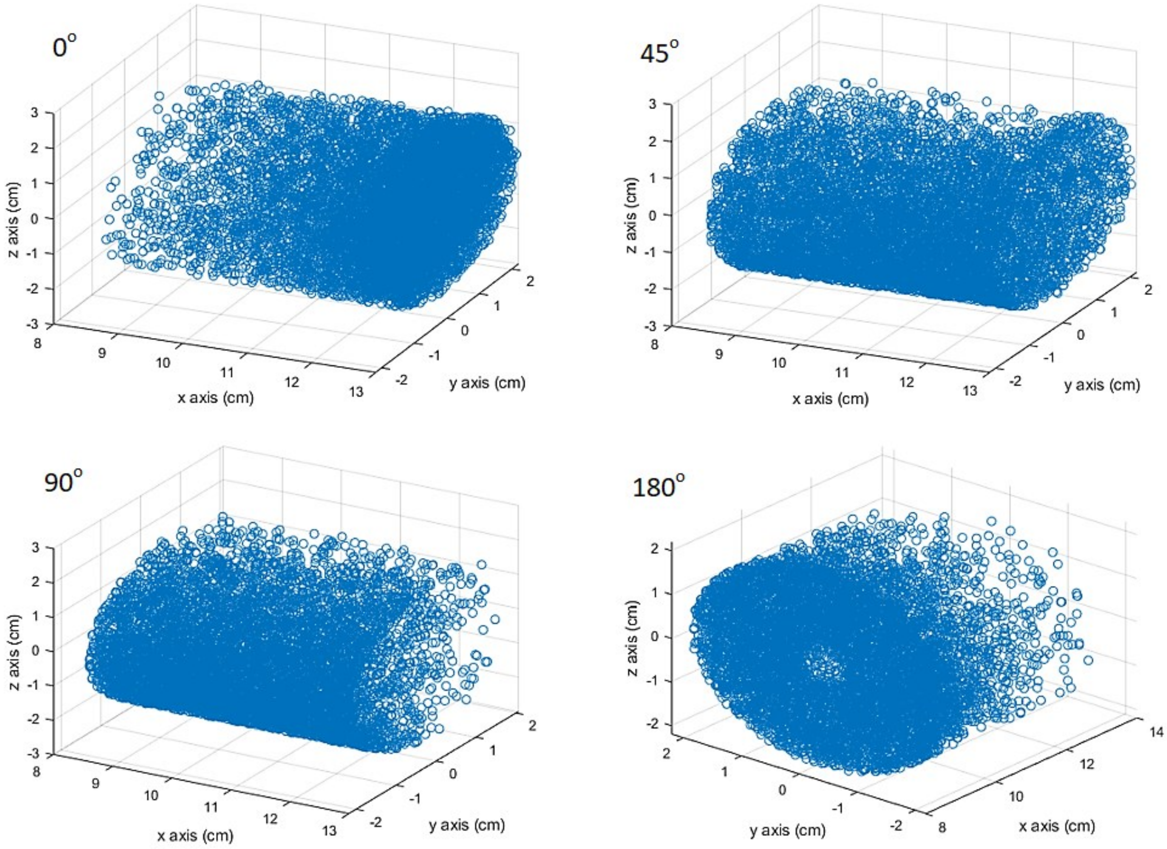

Fig. 5 Gamma energy deposition locations for 10,000 events. 0^0, 45^0, 90^0, 180^0 represent the azimuthal position of the source from the normal of the detector front face. Note that the horizontal axes for 180° are rotated for clarity. These energy deposition locations will have an effect on the resulting pulse shape, which will in turn be represented by the SOM as a specific pattern unique to the source location.

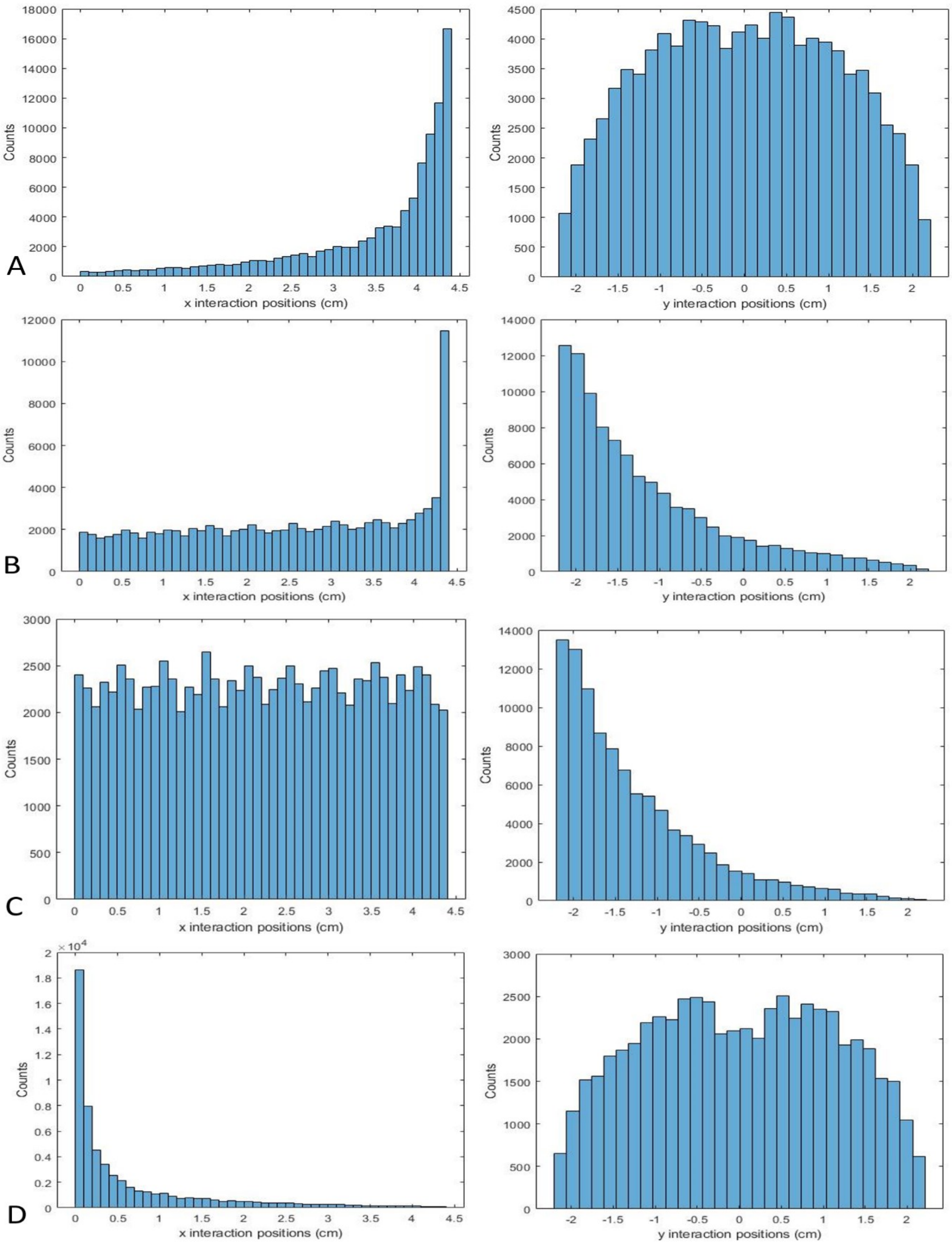

Fig. 6 Intra-detector volume interaction distributions in the x and y directions for a gamma point source located at A) 0^0 B) 45^0 C) 90^0 and D) 180^0 degrees from the normal of the detector front face. The coordinates for the distributions are defined so that the origin is at the radial center and axial base of the detector volume and cold finger, with the x axis pointing towards

the front detector face and the y axis pointing away from the source at 90 degrees. The distributions of the z-coordinates are not shown as the source is not varied in z-plane.

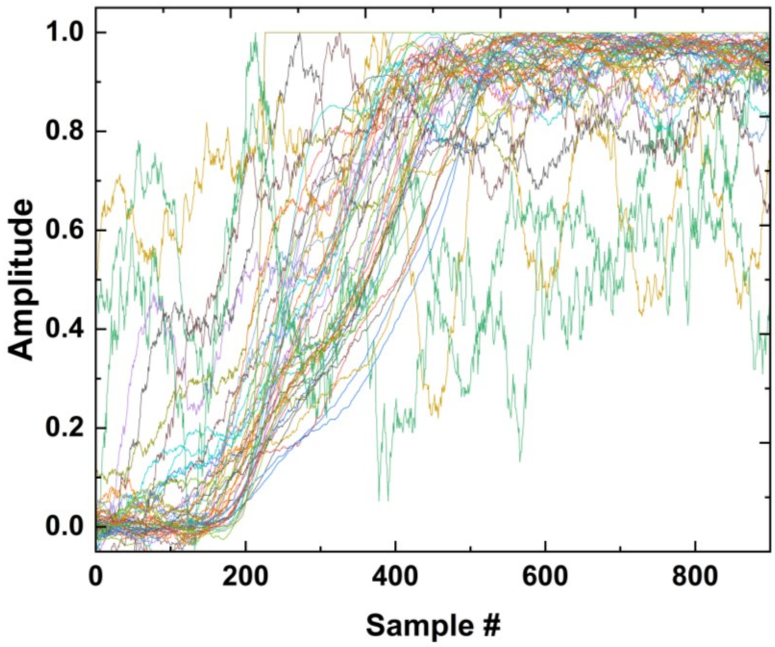

Fig. 7 Normalized pulses collected from the HPGe detector pre-amplifier. The pulses were the inputs to the SOM network. The noisy and saturated pulses were allowed in the training and left in the figure for emphasis on the variety of pulses included in the procedure. These pulses will then be sorted into a specific neuron of the SOM depending on their similarity.

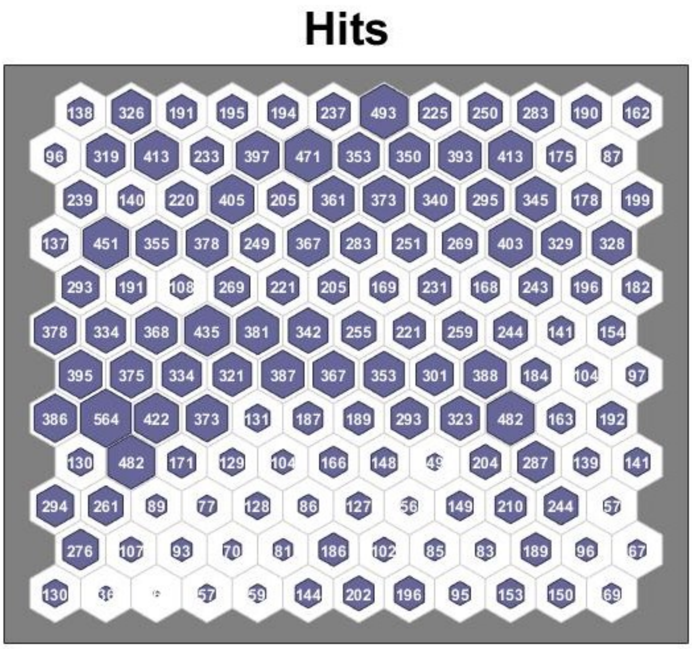

Fig. 8 The sample hits of the trained SOM, which was trained using input pulses collected from all source positions. Each neuron represents a group of pulses with similar characteristics. This trained SOM, when provided a group of pulses originating from a single source location, will then produce a pattern specific to that location.

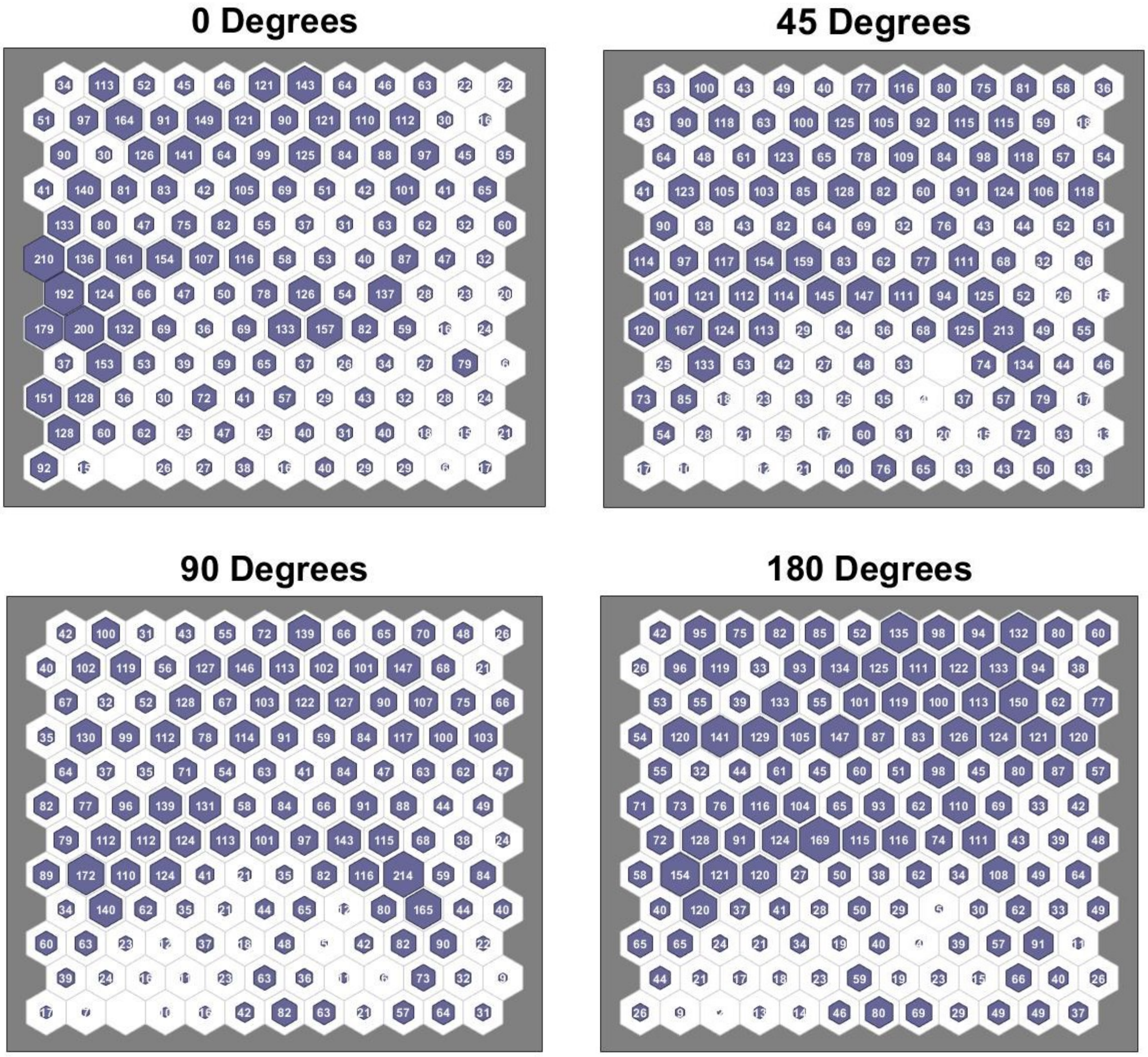

Fig. 9 Representative sample hits of the SOMs produced by the four source positions when 1000 pulses were given to the trained SOM. Each map represents a unique pattern, with some overlap between them. This pattern is consistent across different groups of pulses originating from the same source location, allowing a second neural network to learn to recognize and classify the pattern accordingly.

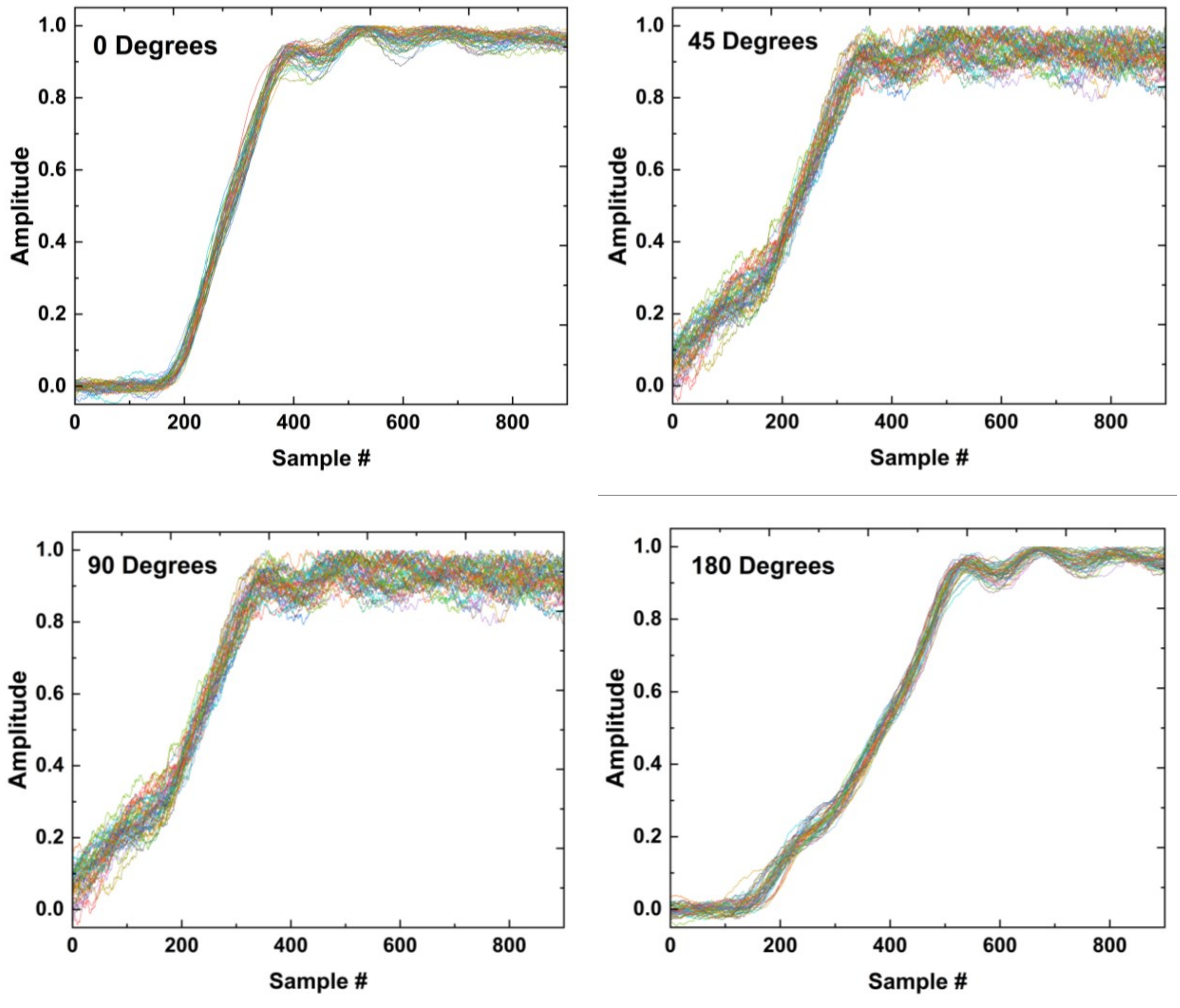

Fig. 10 Example of pulse clusters for the most active neuron in each of the four directional SOMs. Each neuron within the SOM represents a group of pulses with a unique structure—in turn caused by the various locations of gamma energy deposition within the detector.

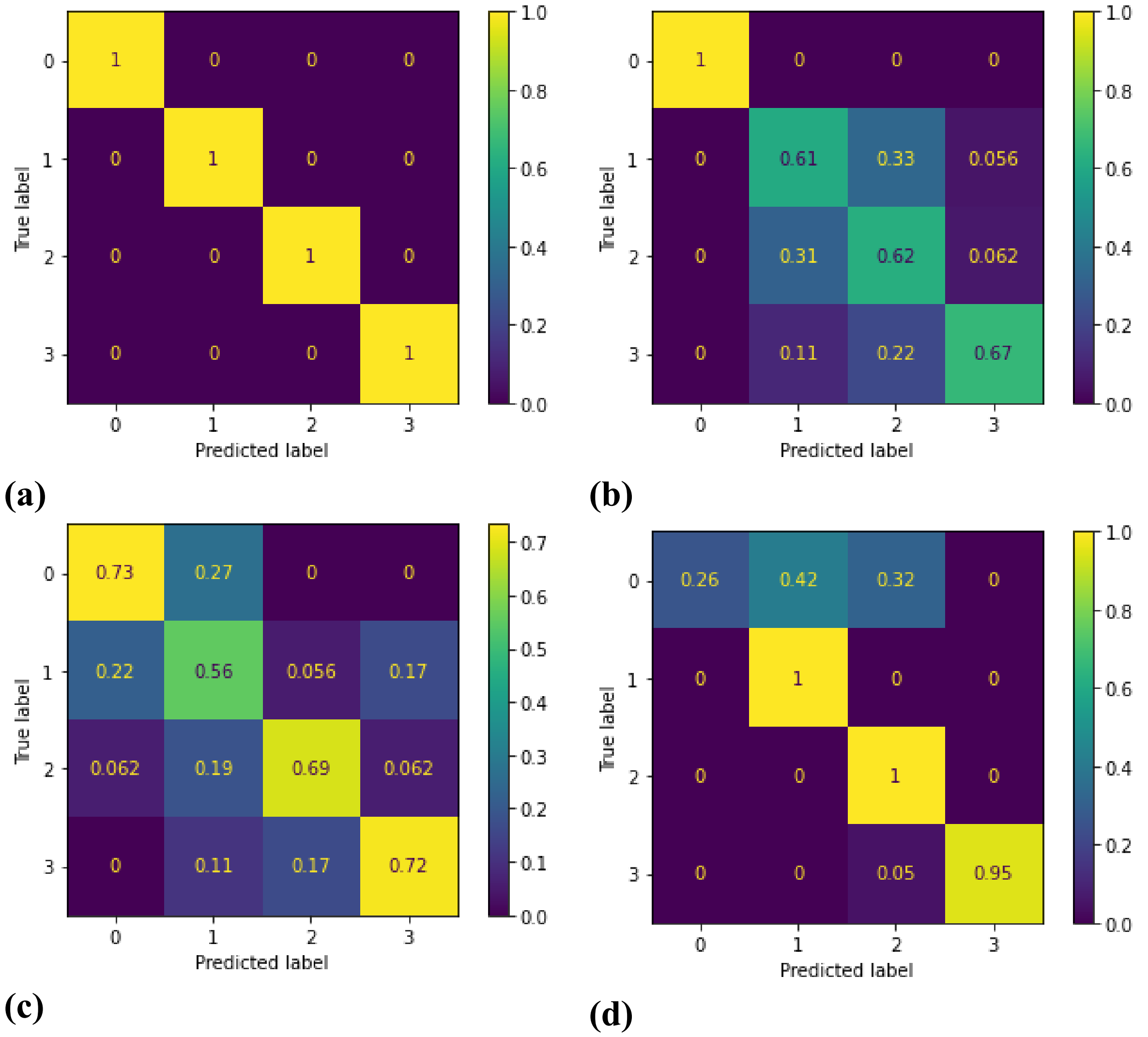

Fig. 11 (a) The confusion matrix of the simple single-layer feedforward model trained on 1000-pulse SOM vectors and tested on 1000-pulse SOM vectors. "1" would represent 100% accuracy. Label 0: 0°; 1: 45°; 2: 90°; 3: 180°. **(b)** The confusion matrix of the model trained and tested on 100-pulse SOM vectors. **(c)** Training set: 1000 pulses per SOM vector; testing set: 100 pulses per SOM vector. **(d)** Training set: 100 pulses per SOM vector; testing set: 1000 pulses per SOM vector.